HELICS GROUP LLC
Scientific Networks

Research Article   **Open Access**

In-Situ Synthesis of Zinc Oxide Nano-Seeds on Muscovite Mica Sheets as A Highly Active Photocatalyst

Anoja Senthilnathan[1], U.G. Mihiri Ekanayake[1], D.M.S.N. Dissanayake[2] and M.M.M.G.P.G. Mantilaka[2*]

[1]Academy of Sri Lanka Institute of Nanotechnology, Nanotechnology and Science Park, Mahenwatte, Pitipana, Homagama, Sri Lanka
[2]Postgraduate Institute of Science, University of Peradeniya, Peradeniya, Sri Lanka

Corresponding author: M.M.M.G.P.G. Mantilaka, Postgraduate Institute of Science, University of Peradeniya, Peradeniya, Sri Lanka, Email: prasanga@pgis.lk, mantilaka@gmail.com

Abstract

Mica is a relatively abundant mineral found on earth's crust and is used in various industries such as paint, construction, electronics, water sciences and so on, due to various properties including softness, lightness, chemical inertness, thermal and electrical stability. This study is an attempt to showcase the potential of value addition to muscovite mica as a photocatalytic agent when a nanocomposite with ZnO is formed. Herein, ZnO nano-layer was deposited on muscovite mica surface and the deposition mechanism was studied. Then this nanocomposite was studied for its photocatalytic degradation ability in the methylene blue dye degradation studies under UV light. The Scanning electron microscopy suggested that the deposited ZnO layer changes its morphology from an oval shape to flower-like morphology when the shape of the mica sheet differs from square to rectangular respectively and the material turns out to be highly reactive against methylene blue dye under UV irradiation having percentage of dye degradation up to 70% per 10 g of the material. This novel material can be used to degrade dye material in an effective, environmentally friendly and cost-effective manner.

Key Words: Zinc Oxide nanoparticles; Nano-surfaces; Photocatalytic degradation; Natural mica surfaces; Photodegradation;

Introduction

Synthesis of nanomaterials and their products using naturally occurring minerals is trending but a young subject area in the fields of nanoscience, geoscience and materials sciences. This effort adds significant value on naturally occurring minerals in a sustainable manner because little quantity of nanomaterials is capable of doing the job which is done by a large quantity of micro- and millimetre-sized particles of the same material. Therefore, small quantities of mineral deposits are required as raw materials for the synthesis of such nanomaterials. As a result, synthesis of nanomaterials is the most sustainable way of adding value to natural minerals and earth resources. Some of the previous works of this discipline include value addition to several minerals such as dolomite, calcite, apatite, magnetite, laterite, quartz and mica [1,2, 3–10, 11,12] by synthesizing various nanomaterials and their products and using these minerals for a broad range of applications.

Mica is a naturally occurring group of sheet silicate minerals that have distinctive perfect cleavage planes parallel to (001) plane. They have the common chemical formula of the repeating unit of $AB_{2-3}(X, Si)_4O_{10}(O, F, OH)_2$ which belongs to the monoclinic crystallographic system and consists of Si_4O_{10} T-O-T layers, interlayered by metal cations. Depending on these cations, mica shows distinctive colour changes and thereby categorized into four main types namely "Lepidolite"- $K(Li, Al)_3(AlSi_3O_{10})(O, OH, F)_2$, "Biotite"- $(Mg, Fe)_3(AlSi3O10)(OH)_2$, "Phlogopite"- $KMg3(AlSi_3O_{10})(OH)_2$, "Muscovite"- $KAl_2(AlSi_3O_{10})(OH)_2$. When considering the properties of mica, it is a relatively soft (Mohr's hardness: 2.5-3), light (specific gravity: 2.76) and flaky material which is transparent to translucent when cleaved along the main cleavage plane. Also, this material is thermally and electrically resistive up to reasonable temperatures and voltages. Because of these properties, mica is used in various industrial applications such as fillers in the construction industry, pigment extenders in the paint industry, additive for drilling

mud in well-drilling industry, electrical insulators in electronic equipment and thermal insulators in various thermal equipment. Due to these industrial applications, mica has a moderately high demand in the mining industry. Mica ores are mainly located and mined throughout the world mainly in Sri Lanka, Russia, Australia, Peru, China, Sweden, Italy and the USA. The study of mica sheets in a water media is recently studied by several authors and the study of the interaction between the aqueous substances and the mica surface shows some special characteristics such as iron exchange properties, time-dependent adsorptive forces and dye adsorption properties [13–16]. Mica is also used to synthesize nanomaterials by depositing various nanoparticles on its surfaces. Zinc oxide is one potential nanoparticle that can grow or attach on mica surfaces to produce photocatalysts and antimicrobial products. ZnO nanoparticles are considered as a very good photocatalytic agent especially in dye degradation [17–22]. However, some applications of photocatalysis limit usage of nanoparticles alone cause some health problems by easy penetration through skin and inhalation. This problem can be avoided by growing or attaching nanoparticles on biocompatible surfaces such as mica.

The objective of current study is to investigate the value addition potential of mica (muscovite) as a photocatalyst in dye degradation. Herein, natural muscovite films are investigated to enhance their photocatalytic activity for methylene blue dye degradation by synthesizing a composite material using ZnO nanoparticles. The study was planned in two different sub-categories. The first half of the study was to synthesize the nanocomposites of muscovite and ZnO nanoparticles including materials characterization. The second part of the study was planned to investigate the photocatalytic activity of the prepared composite. Photocatalytic dye degradation studies were done to investigate the suitable light source (UV or Visible), catalyst dosage and degradation kinetics.

Methods

Materials

Zinc nitrate hexahydrate (purity approx. 99%), cetyltrimethylammonium chloride (CTAC) (with MW of 320 g/mol, purity 99%), sodium hydroxide (NaOH) (purity approx. 98%) and Methylene Blue dye (with MW of 373.90 g/mol) were purchased from Sigma-Aldrich. Mineral mica samples were collected from Matale, Sri Lanka.

Fabrication of Zinc oxide seed nanoparticles growth on thin sheets of muscovite mica (ZnONP-mica)

Thin sheets of mica were cleaved along the natural cleavage plane (001) with an approximate thickness of 200 μm and cut into a desired square shape (0.5 cm × 0.5 cm). 600 μL of CTAC and 50 mL of distilled water were added to a beaker and magnetically stirred for 15 min. Then, 50 mL of 2 M zinc nitrate hexahydrate $(Zn(NO_3)_2 \cdot 6H_2O)$ solution and cut thin-sheets were added with the

above solution and continuously stirred until the solution becomes homogeneous. Later, 50 mL of 4 M NaOH solution was added dropwise in the rate of 1 drop per second for the controlled growth of zinc hydroxide nanoparticles $(Zn(OH)_2$ NPs) on a thin sheet of mica. The solution was continuously stirred for 24 h. Then, the prepared precipitate was washed with distilled water and calcined using muffle furnace at the temperature about 600 °C for 2 h.

Characterization of prepared product material ZnONP-mica

The crystalline structure of the prepared ZnO nanoparticles and ZnONP-mica material and raw material mica were analysed using Bruker Focus D8 Powder X-ray diffractometer (Cu Kα radiation of wavelength λ = 0.1540562 and scan rate 5° min^{-1}). The XRD patterns from Powder X-ray diffractometer was interpreted using the ICDD PDF2 database in X Powder 12 software. The morphologies, average particle size and the aggregates were examined using Hitachi SU6600 field emission scanning electron microscope (FE-SEM) coupled with energy dispersive X-ray (EDX) spectrometer. Samples were also analysed by Bruker Vertex 80 Fourier transform infrared (FTIR) spectrometer under ATR mode. STD Q 600 Simultaneous thermal analyser was used for thermogravimetric analysis of the final product.

Photo-catalytic degradation of industrial standard dye using prepared material

Photo-degradation experiments were carried out in beakers containing 50 mL of Methylene Blue (MB) with a various dose of (1.0, 2.0, 3.0, 4.0 and 10.0 g) synthesized photo-catalyst. The dye-catalyst mixtures were kept under dark conditions for 30 minutes before the photo-irradiation to obtain the adsorption equilibrium and to deduct the possible error due to the adsorption. After that, samples were exposed to UV-C light (257.5 nm) in a sealed box containing two 36 W, low-pressure mercury vapour discharge lamps (Phillips- TUV 36W/G36T8). 3 mL of aliquots were taken out from each sample at 15 min time intervals, centrifuged and UV-Vis spectra were taken by UV-Vis-NIR spectrophotometer (Shimadzu-UV 3600). Percentage degradation amount of MB was calculated by equation (1).

$$Q_e = \frac{(A_0 - A)}{A_0} \times 100 \ \% \qquad (1)$$

Where Qe is the percentage of degradation of dye, A0 is the initial dye concentration and A is the final dye concentration.

The kinetics of each reaction was also determined using second-order kinetics is given by the following equation (2).

$$\frac{1}{[A]} = \frac{1}{[A_0]} + kt \qquad (2)$$

The half-life of this reaction is given by the equations (3).

$$t_{1/2} = \frac{1}{k[A_0]} \qquad (3)$$

Results and Discussions

Characterization of zinc oxide seeds on thin films of mica

The XRD patterns of the raw sample mica, ZnO NPs and ZnO NPs seeds on a thin film of mica are depicted in (Figure: 1). The raw mica sample was confirmed as muscovite with chemical composition as $(K,Na)(Al,Mg,Fe)_2(Si_3Al_{2.90}H_2KO_{12}Si_{3.10})$ (JCPDS card no. 07-0042). The final product ZnO NPs - mica does not show any significant changes in the XRD patterns of natural muscovite except the two weaker peaks at 2θ values of 35.08 and 55.78. This may be due to scattering effects of the ZnO NPs that were grown on mica surface with lower concentration during the analysis of XRD. The chemical composition of the synthesized nanoparticles is confirmed as ZnO in the crystalline form of zincite with hexagonal crystal structure as shown in the (Figure 1) (b) in which entire peaks can be attributed to the positions and the relative intensities of the peak match to the PDF database2 (JCPDS card no. 00-0361451). It consist peaks at 2θ values of 31.54°, 34.48°, 36.48°, 47.8°, 56.82°, 63.1° and 67.72° with corresponding basal planes of (100), (002), (101), (102), (110), (103) and (200) respectively.

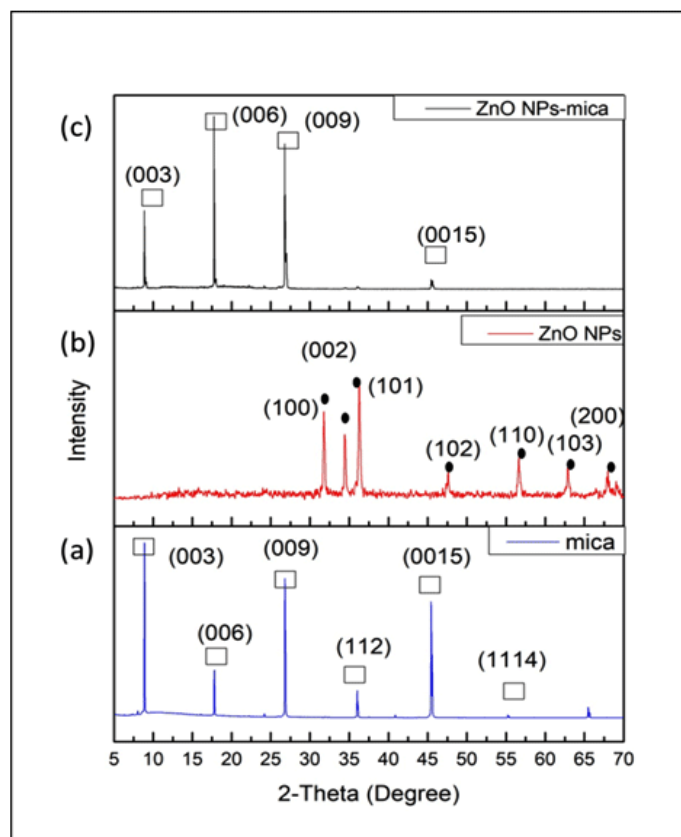**Figure 1:** XRD patterns of (a) mica (b) ZnO NPs (c) ZnO NPs-mica

The chemical structure of the mica, ZnO NPs, intermediate product Zn(OH)2 NPs-mica and final product ZnO NPs-mica are demonstrated in the (Figure 2) (a), (b), (c) and (d) respectively. The FT-IR spectra of $Zn(OH)_2$ NPs-mica and ZnO NPs-mica show a similar pattern like in raw-material muscovite as the compound consists low concentration of NPs on the surface of mica once it compared to natural muscovite. The band around 3424 cm^{-1} due to OH-stretching of the hydroxyl group or water molecule on the surface is invisible in the spectrum of ZnO NPs as the synthetic ZnO NPs are formed after calcination. The peak around 567 cm^{-1} in the spectrum of the ZnO NPs may be attributed to O-H bending of the hydroxyl group. The Zn-O stretching of ZnO is at 431 cm^{-1} is exhibited in the (Figure 2) inset. [23–25]. The FT-IR result shows that intermediate compound has $Zn(OH)_2$ which converts into ZnO during heating step.

The morphology of the ZnO NPs and ZnO NPs seeds on the surface of muscovite (ZnO NPs-mica) are emphasised in the (Figure 3) (a) and (b) respectively with low focus and high focus magnifications. Images of the FE-SEM interpret the presence of the ZnO seeds which were grown on the thin film of muscovite. The dimension of the particles can be seen in the images. The ZnO NPs have oval-shaped morphology with average particle length and width 300 nm and 100 nm respectively. The dimensions of
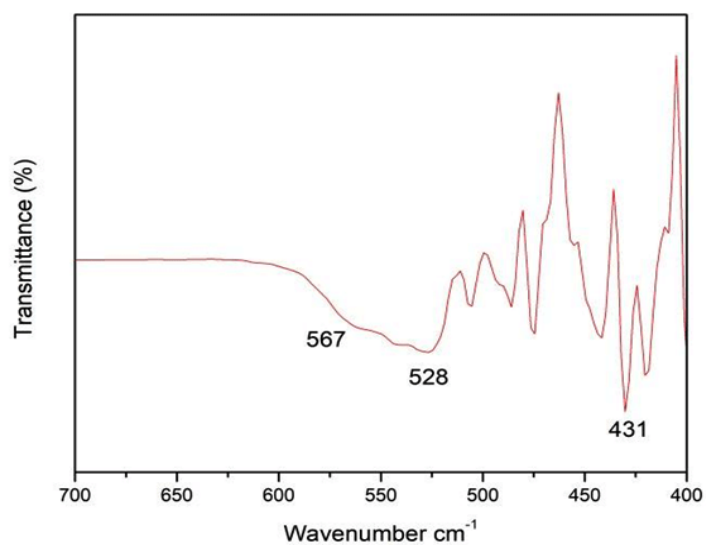
Figure 2: The FT-IR spectra of (a) muscovite (b) Calcined ZnO NPs (c) Zn (OH)$_2$ NPs-mica (d) ZnO NPs-mica (inset represents the FT-IR spectrum of ZnO NPs in the range of 700 cm-1 and 400 cm^{-1})
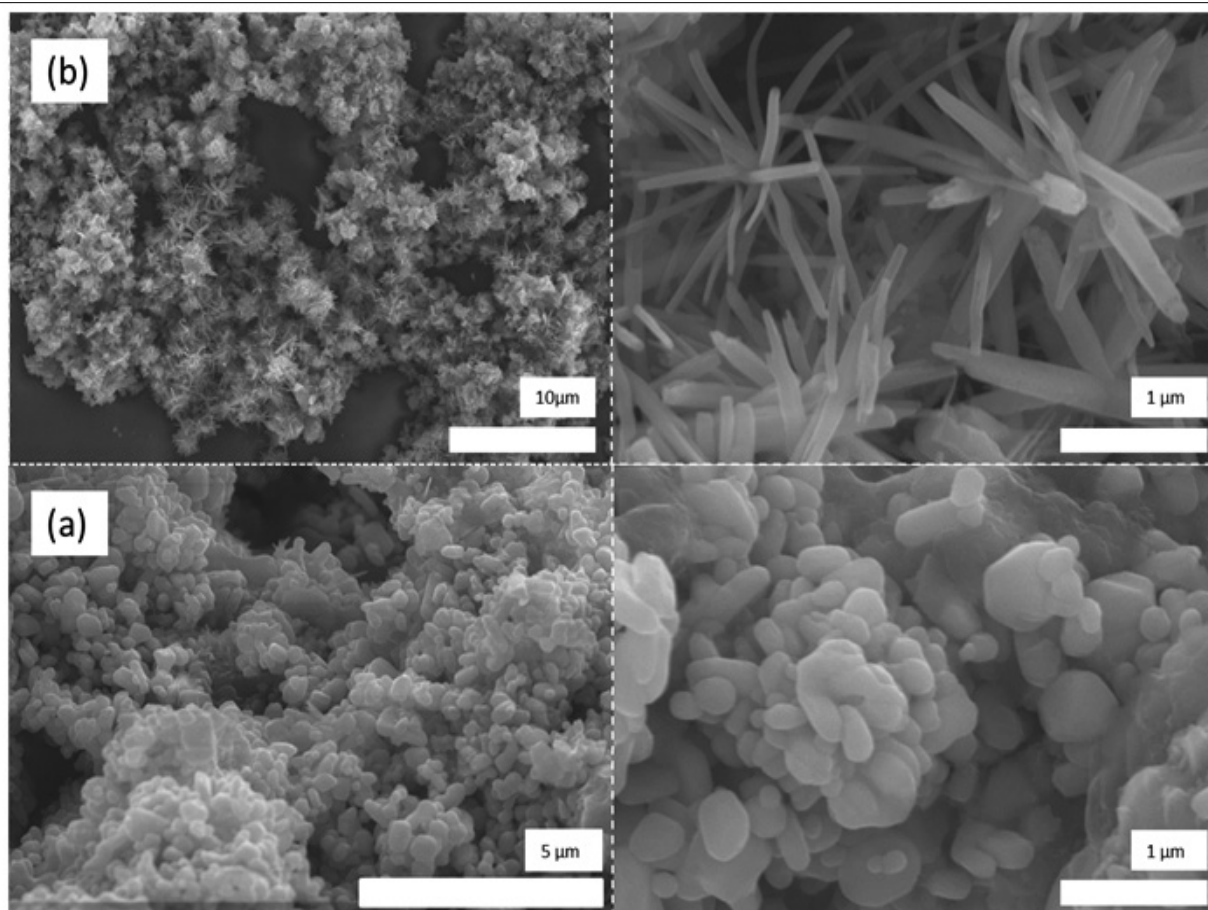

Figure 3: Two different magnifications of (a) ZnO NPs (b) ZnO NPs-mica

the ZnO NPs are not homogenous. The FE-SEM images confirmed the transformation of the morphology to a flower-like structure when the seeds were grown on a thin film of mica with elongated length and shortened width. The average length and width of the ZnO NPs which were grown on the surface of mica are 1 μm and 50 nm respectively. Even though, the individual ZnO NPs show less homogeneity, ninety per cent of the ZnO NPs are homogenous and evenly distributed all over the surface of the muscovite film.

The TGA graphs of the ZnO NPs, natural raw material muscovite and ZnO NPs-mica are exhibited in (Figure 4) to interpret the thermal stability of these materials. The mass-loss of 0.6% of ZnO NPs occurs at around 100°C- 350 °C is due to the removal of adsorbed water on to the sample as shown in (Figure 4). Muscovite and ZnO NPs-mica show a similar trend of TGA curves which are demonstrated in the Fig.4. Even though they show the same behaviour, there is

also a significant difference between muscovite and ZnO NPs-mica at the range 200°C to 800°C which can be seen in the focused in the image. The muscovite shows higher thermal stability than the product ZnO NPs-mica. The mass-loss for muscovite and ZnO NPs-mica at the temperature between 150°C to 400°C as 0.5% and 0.9% are due to adsorbed water which is different from simple moisture. The mass loss for ZnO NPs-mica lowers due to the lower concentration of ZnO NPs on the surface of the mica. The total mass loss at the temperature 980°C corresponding to muscovite and ZnO NPs-mica are about 4.7% is explained as the most of the removal of hydroxyl ions below the temperature 850°C [26]. Dehydroxylation of muscovite has taken place at a wide range of temperature (780 –950°C) during dynamic and static heating [27]. The TGA curves of the ZnO NPs, muscovite and ZnO NPs-mica ensure that these materials are thermally stable enough up to the temperature of 1000°C.
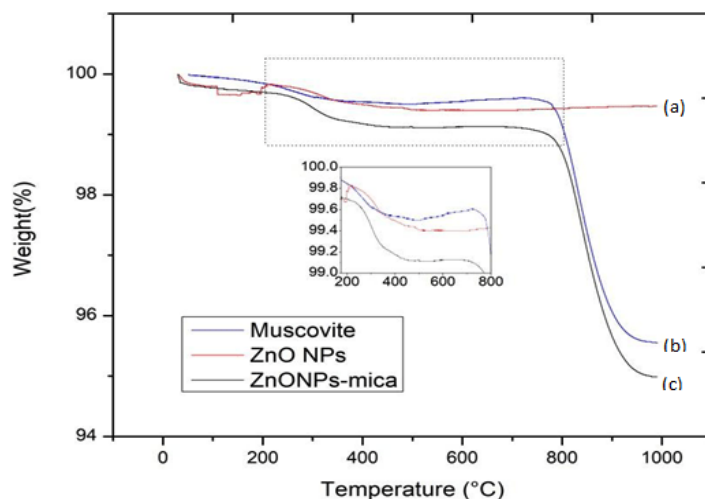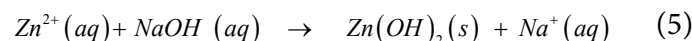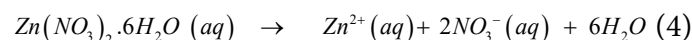

Figure 4: TGA plots of (a) ZnO NPs, (b) Muscovite mica and (c) ZnO NPs –mica

Elemental composition of the prepared material (ZnO NPs-mica) is determined by EDX elemental map as depicted in (Figure 5) with EDX spectrum. EDX map describes that the prepared material composed of elements of the muscovite (K, Al, Si, O) and the components of ZnO NPs (Zn, O) with their weight percentages of the coverage area. The EDX map confirms that 45.3 % of zinc have distributed on the surface of mica as representative coverage of the material.

Seeds of ZnO NPs were grown on the surface of mica by the *in-situ* technique where the nanoparticles were distributed on the substrate at the time of formation of the nanoparticles. In this reaction process, silicate layered muscovite act as a negatively surface charged substrate for the growth of the nanoparticles. cetyltrimethylammonium chloride (CTAC) is the cationic surfactant was added at the initial stage of reaction to control the size and shape of the nanoparticles and maintain the stability of the products from agglomeration.

The chemical reaction of growth of ZnO nanoparticles as follows:

$$Zn(NO_3)_2.6H_2O\ (aq)\quad \rightarrow \quad Zn^{2+}(aq)+ 2NO_3^-(aq)\ +\ 6H_2O\ (4)$$

$$Zn^{2+}(aq)+ NaOH\ (aq)\quad \rightarrow \quad Zn(OH)_2(s)\ +\ Na^+(aq)\qquad (5)$$

The nanoparticles can be stabilized by the capping agent CTAC as it inhibits the collision of nanoparticles that can be resulted in aggregation.

These cationic sites of formed nanoparticles will be interacting with negatively surface charged muscovite surface due to electrostatic interaction.

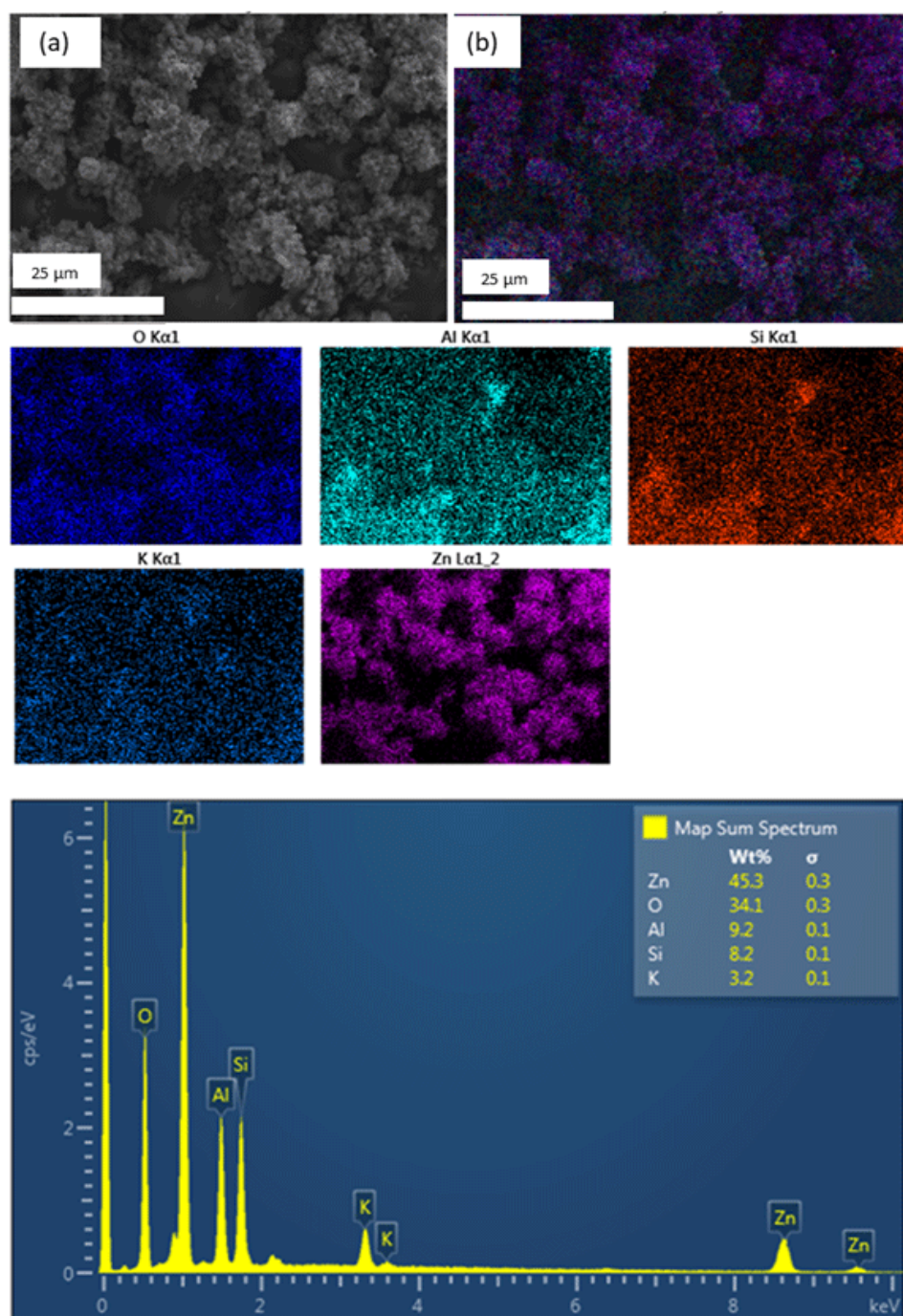The reaction after calcination to 600°C

$$Zn(OH)_2\ NPs\ -mica\quad \rightarrow\ ZnO\ NPs-mica\qquad (6)$$
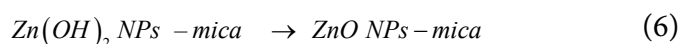
Figure 5: EDX mapping and spectrum of ZnO NPs-mica

The surfactant CTAC was completely removed by washing the product several times and calcination process with decomposing as CO_2 and H_2O [28].

Photo-catalytic property of prepared product ZnO NPs-mica

Catalytic activity of the material is expected to be enhanced due to the high surface area of the material and properties of the surface. This can be further explained by the terms of high concentration of active sites on the surface and high organic dye molecules absorbed on to the nanometer scale catalytic surface. The electrons in the valence band (VB) of ZnO NPs-mica have been excited to the conduction band (CB) by leaving holes in the VB. Photoinduced electrons can react with oxygen absorbed to the material surface or oxygen dissolved in the water. This reduction process creates superoxide radicals ($\bullet O_2$) which can help the degradation process. The adsorbed water molecules on surfaces of ZnO NPs and mica play a major role in the formation of hydroxyl radicals ($\bullet OH$) through the

reaction with photo-generated holes or superoxide radicals at the surface of the photocatalyst [29]. Furthermore, these oxygen free radicals react with H+ and produce hydroperoxyl radicals (•OOH) and H2O2. Moreover, further reduction mechanism can be occurred by providing (•OH) [30–32]. These free radicals formed during the process degrade the model organic dye which is a pollutant and releases CO2 and H2O as non-harmful products. The photo-degradation of methylene blue follows the following reactions and steps of mechanism:
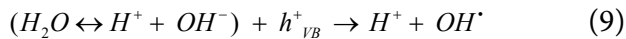
1. Absorption of required photon energy by the photo-catalyst ANPM

$$ZnO\ NPs-mica\ +\ hv \rightarrow e^-_{CB} + h^+_{VB} \qquad (7)$$
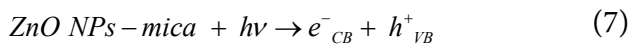
2. Superoxide formation through an oxygen reduction reaction

$$O_2\ +\ e^-_{CB} \rightarrow O_2^{\bullet\,-} \qquad (8)$$

3. Highly reactive OH• formation from water molecules

$$(H_2O \leftrightarrow H^+ + OH^-)\ +\ h^+_{VB} \rightarrow H^+ + OH^{\bullet} \qquad (9)$$

4. Neutralization of superoxide

$$O2^{\bullet-} + H^+ \rightarrow HO_2^{\bullet} \qquad (10)$$

5. Formation of Hydrogen peroxide

$$2\ HO_2^{\bullet} \rightarrow H_2O_2\ +\ O_2 \qquad (11)$$

6. Formation of highly reactive OH• radicals

$$H_2O_2 + e^-\ \rightarrow OH^{\bullet} +\ OH^- \qquad (12)$$

7. Degrading of the methylene blue

$$R\ (methylene\ blue) + OH^{\bullet} \rightarrow\ R^{\bullet} + H_2O \qquad (13)$$

$$R\ +\ h^+\left(hole\right) \rightarrow R^{+\bullet} \rightarrow Degradation\ Products \qquad (14)$$

8. End Reaction

$$RCOO^- + h^+\left(hole\right)\ \rightarrow\ R^{\bullet} +\ CO_2 \quad [23,24] \qquad (15)$$
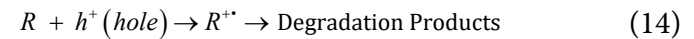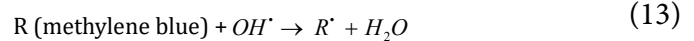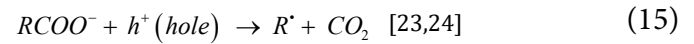
The effects of catalyst (ZnO NPs-mica) dosage and irradiation time on the percentage degradation of MB aqueous solution under UV-C light have been illustrated in (Figure 6). The maximum absorbance of MB is observed around 663 nm in the UV-Vis spectra. The reduction of absorbance as a function of time can be attributed to the photo-degradation of the model organic dye compound by the synthesized material. The UV–vis spectra do not show any significant variation of the absorbance value after keeping under the dark condition compared to the initial dye solution. The percentage degradation versus time plot describes that the photo-catalytic dye degradation increases with increasing catalyst dosage. The observed photo-catalytic dye degradation percentages for 1.0, 3.0, 4.0 and 10.0 g of synthesized materials are 26.5%, 42%, 48.2% and 70% under UV exposure within 210 min respectively. The graph confirms the significant dye degradation under UV exposure using synthesized photo-catalyst. Finally, when degradation completes all methylene blue dye converts into CO_2 and H_2O. Therefore, no radicals of dyes remain in the solution. The material can be applied at the bottom and surfaces of water/waste treatment plants which is one of advantages of using mica surface. Therefore, this material is reusable and the treatment tank can degrade organic materials again and again.
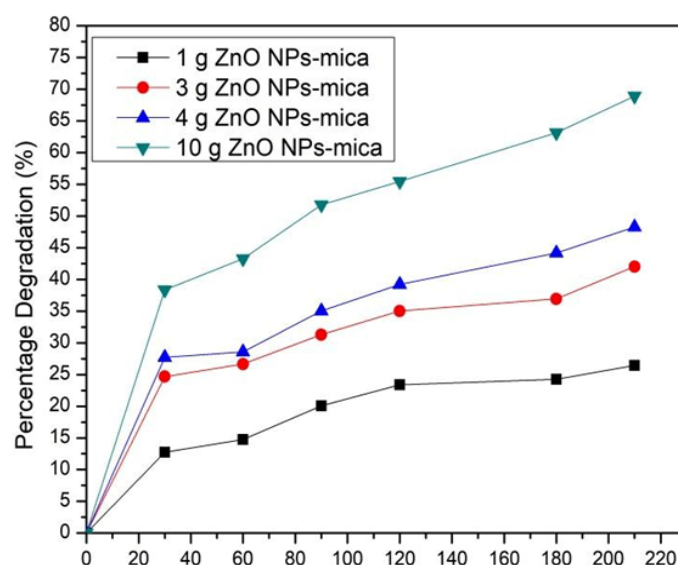

Figure 6: Percentage degradation of 5 ppm MB dye with different catalyst dosages of ZnO NPs-mica with time, under UV-C light

The comparison of the catalyst dosage (3.0 g) ZnO NPs-mica over time with varying the sources of irradiation as UV-C light and visible light is demonstrated in (Figure 7). About 42.0 % and 21.2 % of the dye solution has been degraded by 3.0 g (±0.01) of ZnO NPs -mica within 210 min under UV-C light and visible light respectively. This graph affirms that the higher degradation efficiency of the novel material is observed under UV-C light than the visible light.

The plots of 1/C versus irradiation time under UV-C light and visible light are shown in (Figure 8) (a) and (b) respectively to interpret the kinetics of the photocatalytic reaction. These graphs explain that the MB degradation by synthesized material follows second-order kinetics under UV-C light. The rate constant (k), half-life (t 1/2) and linear coefficient (R2) under UV-C light are 0.00187 min^{-1}, 107 min and 0.966563 respectively. The same parameters under visible light are 4.2644 E-4, 2.564 min and 0.73076 respectively. It can be concluded with data of MB dye percentage degradation that photo-catalyst effectively degrade the dye with a short time under UV-C light.
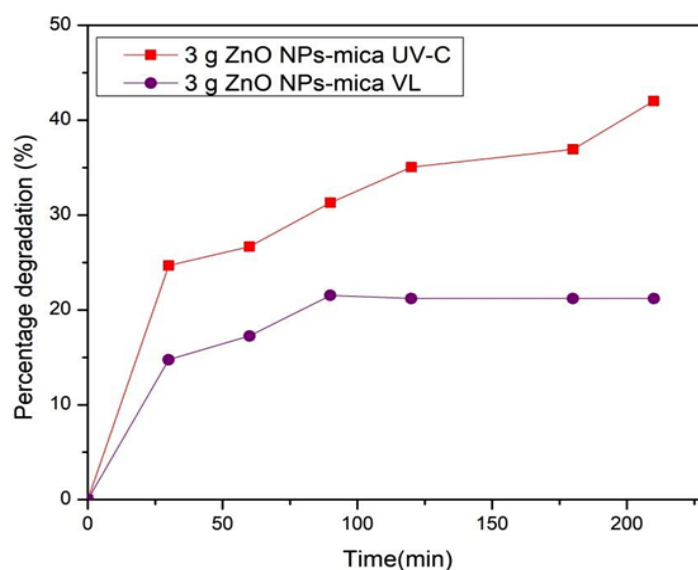

Figure 7: Percentage degradation of 5 ppm MB dye by 3 g of catalyst dosage with different source of irradiation UV-C light and Visible light with time
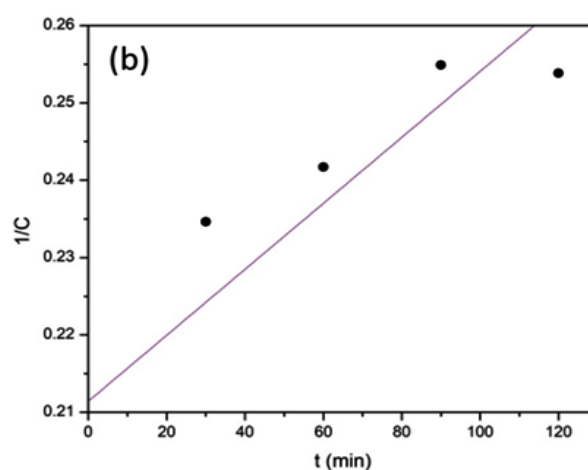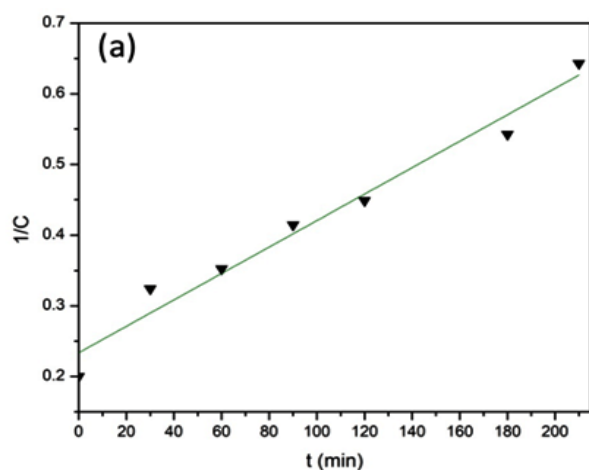

Figure 8: Kinetics of photo-catalytic reaction (a) UV-C light (b) Visible light

Conclusions

Synthesis of ZnO nanoparticle seed has been attached to naturally occurring mica surfaces well. In here, the micelles of CTAC in which the $Zn(OH)_2$ particles form attracts to the mica surface because of the surficial attractive forces of mica and get deposited. Upon calcination, the micelle has decomposed away and the ZnO particles are revealed. In the MB dye degradation studies, both materials contribute to the mechanism where the mica surface attracts the dye molecule and provides an easy path to photodegrade the dye molecules more effectively. The material is thermally stable. The final material can be applied on bottom and surfaces of water treatment plants to degrade dyes and many other organic pollutants by photo-degradation under sunlight or UV radiation. As the materials are green and mica is readily available, the final product is cost-effective. Therefore, the synthesized ZnO nanoparticles deposited mica surfaces have a good potential to be used in cost effective dye effluent treatment plants by complete photodegradation.

Acknowledgement

References

1. Wijesinghe WPSL, Mantilaka MMMGPG, Karunarathne TSEF, Rajapakse RMG. Synthesis of a hydroxyapatite/poly(methyl methacrylate) nanocomposite using dolomite. Nanoscale Adv. 2019;1:86–88. doi:10.1039/c8na00006a

2. Priyadarshana G, Kottegoda N, Senaratne A, De Alwis A and Karunaratne V. Synthesis of magnetite nanoparticles by top-down approach from a high purity ore. J Nanomater. 2015;1–8. doi:10.1155/2015/317312

3. Mantilaka M, Wijesinghe W, Pitawala H, Rajapakse RMG, Karunaratne D. Surfactant-assisted synthesis of pure calcium carbonate nanoparticles from Sri Lankan dolomite. J Natl Sci. Found. 2014;42(3):221-228.

4. Mantilaka M, Rajapakse RMG, Karunaratne D, Pitawala H. Preparation of amorphous calcium carbonate nanoparticles from impure dolomitic marble with the aid of poly (acrylic acid) as a stabilizer. Adv. Powder Technol. 2014;25:591–598.

5. Mantilaka M, Karunaratne D, Rajapakse RMG, Pitawala H. Precipitated calcium carbonate/poly (methyl methacrylate) nanocomposite using dolomite: synthesis, characterization and properties. Powder Technol. 2013;235:628–632.

6. Mantilaka MMMGPG, Rajapakse RMG, Karunaratne DGGP, Pitawala HMTGA. Preparation of amorphous calcium carbonate nanoparticles from impure dolomitic marble with the aid of poly(acrylic acid) as a stabilizer. Adv. Powder Technol. 2014;25(2):591-598. doi:10.1016/j.apt.2013.09.008

7. Mantilaka MMMGPG, Pitawala HMTGA, Karunaratne DGGP, Rajapakse RMG. Nanocrystalline magnesium oxide from dolomite via poly(acrylate) stabilized magnesium hydroxide colloids. Colloids Surfaces A Physicochem Eng Asp. 2014;443:201-208. doi:10.1016/j.colsurfa.2013.11.020

8. Dissanayake DMSN, Mantilaka MMMGPG, De Silva RT, Pitawala HMTGA, Nalin De Silva KM and Amaratunga GAJ. Cost effective, industrially viable production of Fe2O3 nanoparticles from lat-erites and its adsorption capability. Mater Res Express. 2019;6. doi:10.1088/2053-1591/ab3ce5

9. Dissanayake DMSN, Mantilaka MMMGPG, Palihawadana TC, Chandrakumara GTD, De Silva RT, Pitawala HMTGA, Nalin de Silva KM, Amaratunga GAJ. Facile and low-cost synthesis of pure hematite (α-Fe 2 O 3) nanoparticles from naturally occurring laterites and their superior adsorption capability towards acid-dyes. RSC Adv. 2019;9:21249-21257. doi:10.1039/C9RA03756J

10. Chandrakumara GTD, Dissanayake DMSN, Mantilaka MMMGPG, De Silva RT, Pitawala HMTGA and de Silva KMN. Eco-Friendly, Green Packaging Materials from Akaganeite and Hematite Nanoparticle-Reinforced Chitosan Nanocomposite Films. J. Nanomater. 2019;1–11. doi:10.1155/2019/1049142

11. Senthilnathan A, Dissanayake DMSN, Chandrakumara GTD, Man-tilaka MMMGPG, Rajapakse RMG Pitawala HMTGA and Nalin de Silva KM. Akaganeite nanorices deposited muscovite mica surfaces as sunlight active green photocatalyst. R Soc Open Sci. 2019;6:182212. doi:10.1098/rsos.182212

12. Wijesinghe WPSL, Mantilaka MMMGPG, Rajapakse RMG, Pitawala HMTGA, Premachandra TN, Herath HMTU, Rajapakse RPVJ, and Wijayantha KGU. Urea-assisted synthesis of hydroxy-apatite nanorods from naturally occurring impure apatite rocks for biomedical applications. RSC Adv. 2017;7: 24806-24812. doi:10.1039/c7ra02166f

13. Gaines GL. The ion-exchange properties of muscovite mica. J. Phys. Chem. 1957;61:1408–1413. doi:10.1021/j150556a033

14. Fischer D, Caseri WR, Hähner G. Orientation and electronic structure of ion exchanged dye molecules on mica: An x-ray absorption study. J. Colloid Interface Sci. 1998;198:337–346. doi:10.1006/jcis.1997.5296

15. Okada T, Ehara Y, Ogawa M. Adsorption of Eu3+ to smectites and fluoro-tetrasilicic mica. Clays Clay Miner. 2007;55(4):348–353. doi:10.1346/CCMN.2007.0550402

16. Karthaus O, Kawatani Y. Self-assembly and aggregation control of cyanine dyes by adsorption onto mesoscopic mica flakes.

Japanese J. Appl. Physics, Part 1 Regul. Pap. Short Notes Rev Pap. 2003;42:127–131. doi:10.1143/JJAP.42.127

17. Akyol A, Yatmaz HC, Bayramoglu M. Photocatalytic decolorization of Remazol Red RR in aqueous ZnO suspensions. Appl Catal. B Environ. 2004;54:19–24. doi:10.1016/j.apcatb.2004.05.021Zheng Y, Zheng L, Zhan Y, Lin X, Zheng Q, Wei K. Ag/ZnO heterostructure nanocrystals: Synthesis, characterization, and photocatalysis. Inorg Chem. 2007; 46: 6980–6986. doi:10.1021/ic700688f

18. Zheng Y, Zheng L, Zhan Y, Lin X, Zheng Q, Wei K. Ag/ZnO heterostructure nanocrystals: Synthesis, characterization, and photocatalysis. Inorg Chem. 2007; 46: 6980–6986. doi:10.1021/ic700688f

19. Li D, Haneda H. Morphologies of zinc oxide particles and their effects on photocatalysis. Chemosphere, 2003 ;51:129–137. doi:10.1016/S0045-6535(02)00787-7

20. Sakthivel S, Neppolian B, Shankar M V., Arabindoo B, Palanichamy M, Murugesan V. Solar photocatalytic degradation of azo dye: Comparison of photocatalytic efficiency of ZnO and TiO2. Sol. Energy Mater. Sol. Cells. 2003;77:65–82. doi:10.1016/S0927-0248(02)00255-6

21. Li B, Wang Y. Synthesis, microstructure, and photocatalysis of ZnO/CdS nano-heterostructure. J. Phys. Chem. Solids 2011;72:1165–1169. doi:10.1016/j.jpcs.2011.07.010

22. Yang JL, An SJ, Park W Il, Yi GC, Choi W. Photocatalysis using ZnO thin films and nanoneedles grown by metal-organic chemical vapor deposition. Adv Mater. 2004;16:1661–1664. doi:10.1002/adma.200306673

23. Saoud K. Prevention of hospital infections using Ag/ZnO nanoparticle visible light photocatalyst. Qatar Found. Annu Res Forum Proc. 2013;2013:BIOP 037. doi:10.5339/qfarf.2013.biop-037

24. Suwanboon S. Structural and optical properties of nanocrystalline ZnO powder from sol-gel method. ScienceAsia. 2008;34:31–34. doi:10.2306/scienceasia1513-1874.2008.34.031

25. Thirugnanam T. Effect of polymers (PEG and PVP) on sol-gel synthesis of microsized zinc oxide. J. Nanomater. 2013;2013:7. doi:10.1155/2013/362175

26. Gridi-Bennadji F, Beneu B, Laval JP, Blanchart P. Structural transformations of Muscovite at high temperature by X-ray and neutron diffraction. Appl Clay Sci. 2008;38:259–267. doi:10.1016/j.clay.2007.03.003

27. Kodama H, Brydon JE. Dehydroxylation of microcrystalline muscovite. Kinetics, mechanism and energy change. Trans. Faraday Soc. 1968;64:3112–3119. doi:10.1039/TF9686403112

28. Zhang Z, Mayoral A, Melián-Cabrera I. Protocol optimization for the mild detemplation of mesoporous silica nanoparticles resulting in enhanced texture and colloidal stability. Microporous Mesoporous Mater. 2016;220:110–119. doi:10.1016/j.micromeso.2015.08.026

29. Reza Gholipour M, Dinh C-T, Béland F, Do T-O. Nanocomposite heterojunctions as sunlight-driven photocatalysts for hydrogen production from water splitting. Nanoscale. 2015;7:8187–8208. doi:10.1039/C4NR07224C

30. Sun Z, Li L, Li J, Zheng H, Luo W. Influence of Nb2O5 addition on dielectric properties and diffuse phase transition behavior of BaZr0.2Ti0.8O3 ceramics. Ceram Int. 2016;42:10833–10837. doi:10.1016/j.ceramint.2016.03.212

31. Ibhadon AO, Fitzpatrick P. Heterogeneous photocatalysis: Recent advances and applications. Catalysts. 2013;3:189–218. doi:10.3390/catal3010189

32. Hojamberdiev M, Katsumata KI, Matsushita N, Okada K. Preparation of Bi_2WO_6- and BiOI-allophane composites for efficient photodegradation of gaseous acetaldehyde under visible light. Appl. Clay Sci. 2014;101:38–43. doi:10.1016/j.clay.2014.07.007